MULTIBODY DYNAMICS 2011, ECCOMAS Thematic Conference
J.C. Samin, P. Fisette (eds.)
Brussels, Belgium, 4-7 July 2011

DEVELOPMENT OF AN INNOVATIVE MODEL FOR THE EVALUATION OF WHEEL WEAR IN RAILWAY VEHICLES

Jury Auciello*, Mirko Ignesti*, Enrico Meli* and Andrea Rindi*

*Department of Energy Engineering
University of Florence, Via S. Marta n. 3, 50139 Firenze, Italy
e-mails: auciello@mapp1.de.unifi.it, ignesti@mapp1.de.unifi.it,
meli@mapp1.de.unifi.it, rindi@mapp1.de.unifi.it,
web page: http://www.unifi.it/mdmlab

Keywords: wheel-rail wear evaluation, wheel-rail contact modeling, multibody simulations

Abstract. *In railway applications, the estimation of the wear in the wheel-rail contact is an important field of study, mainly correlated to the planning of maintenance interventions, vehicle stability and the possibility to carry out specific strategies for the wheel profile optimization. In this work Authors present a model conceived for the evaluation of the wheel profile evolution due to wear, which is organized in two parts, mutually interactive: a vehicle model for the dynamic analysis and a model for the wear estimation. The first one is a 3D multibody model of a railway vehicle implemented in SIMPACK™, a commercial software for the analysis of mechanical systems; the wheel-rail interaction, based on an innovative contact points research method developed by Authors in previous works, is implemented in a C/C++ user routine of SIMPACK. Normal and tangential forces in the contact patches are calculated according to Hertz and Kalker's global theory respectively. The wear model, developed in MATLAB® environment, is based on the abrasive wear and the Reye hypothesis. It starts from the outputs of the multibody simulations (position of contact points, contact forces and creepages) and estimates the contact pressures by means of a local contact model (FASTSIM algorithm); finally the worn material is calculated through the Reye hypothesis. This approach allows, evaluating both the quantity of removed material and its distribution along the wheel profile, to analyze the development of the wheel shape during its lifetime. In order to reproduce the wear progression, the overall mileage traveled by the vehicle is divided into discrete steps during which the wheel profile is constant; after simulating one step, the wheel profile is updated by means of the wear model. Therefore, the two models work alternately until completing the whole mileage. The choice of an appropriate length of the step is fundamental in terms of precision and computational time required. The entire model has been validated in collaboration with Trenitalia S.p.A, which has provided the technical documentation and the experimental results relating to some tests performed with the vehicle ALn 501 "Minuetto" on the Aosta-Pre Saint Didier line.*

1 Introduction

In the railway field, the availability of a mathematical model for the prediction of the wear in the wheel-rail contact represents a powerful tool for different reasons. First of all, the estimation of the wear rate turns out to be very important to plan the maintenance interventions. In fact, as the wear proceeds, the shape of the wheel profiles evolves leading to variations of the performance both in negotiating curves and in running stability on straight tracks; so the original profiles should be periodically re-established by means of turning. Especially from a safety viewpoint, the development of a contact geometry which may compromise the vehicle stability or increase the derailment risk should be avoid. As a matter of fact, vehicle instability could appear even at low speeds in case of high equivalent conicity in the wheel-rail coupling, whereas the derailment may be facilitated by low flange contact angles.

A reliable wear model can also be used to optimize the original wheel profile to guarantee a uniform wear, that is stable geometric characteristics of the contact geometry during the use of the wheel. In this way the overall amount of removed material may be reduced, hence the mean time between two maintenance interventions could raise as well as the performance of the wheel-rail contact may be kept approximately constant between two turnings.

It is important to underline that one of the most critical aspect in the development of a wear model is the availability of experimental results, since the wear is a long-term phenomenon which requires some months to collect sufficient data. In addition, for a correct interpretation of the data, they must be opportunely stratified to correlate the influent factors (vehicles characteristics, tracks, rail conditions, etc) to the wear evolution. If on line experimental measurement cannot be carried out, the problem could be faced using tools provided by softwares or carrying out experimental proofs on a scaled test rig.

In this work, Authors will present a procedure to estimate the evolution of the wheel profile due to wear by means of a model that involves multibody simulations and the use of wear model. More precisely, the general layout adopted is made up of four parts mutually interactive: the vehicle model (multibody model and wheel-rail global contact model) and a wear model (local contact model and wear evaluation using the Reye hypothesis). The multibody model, implemented in SIMPACK, is an accurate dynamic representation of the motion of the vehicle which takes into account all the significant degrees of freedom. The global contact model, developed in previous works [7], calculates the contact forces between the wheelset and rail and interacts online with the multibody model to reproduce the vehicle dynamics; in particular, it uses an innovative algorithm in the research of the contact points between the wheelset and the rail, with a three-dimensional approach to the problem. In regard to the wear model, it is based on the FASTSIM local contact model and on the Reye hypothesis; it uses the outputs of the multibody simulations to calculate the amount of removed material and its distribution along the wheel profile. The removal of material is carried out considering the three-dimensional structure of the phenomenon.

The entire model has been validated utilizing the available experimental data provided by Trenitalia S.p.A. and Rete Ferroviaria Italiana, relative to the Aosta-Pre Saint Didier railway line and the Aln 501 “Minuetto” which exhibits seriuos problems in terms of wear in this scenery.

2 General Architecture of the Model

The layout of the whole model has been developed on the basis of the following working hypothesis, agreed with Trenitalia S.p.A:

- the track is not subjected to wear and the rail profiles are always kept constant;

- the unique wear mechanism is the abrasion;
- dry conditions are assumed in the wheel-rail contact;
- the wheel profiles are the same for each vehicle's wheel and the output of the wear model is the evolution of a single mean wheel profile, which comprises the effects of the wear on all the vehicle's wheels.

Since the wear is a long-term phenomenon which requires at least ten of thousand kilometers (but even hundreds of kilometers in the most cases) to express its effects, the simulated distances are obviously shorter than the real ones which have to be investigated. The almost linear trend of the wear as a function of the traveled distance assures a simple correlation between the two distances, based on an opportune proportionality, as long as the simulations are a significant representation of the real traveled distance, as it will be explained below. In addition, the numerical evolution of the wheels geometry is not a continuous process, but is treated with a discrete approach. The entire mileage to be simulated is divided in a few steps, in which the wheel profiles are maintained constant throughout the simulations; on the base of the results of the following wear evaluation, at the end of each step the wheels profiles are updated for the next simulations set. The length of this spatial step is one of most important aspect of the entire numerical procedure: in fact, the longer the step is, the higher the accuracy and the overall computation time are, hence, the choice of the step length has to be done as a compromise between these aspects.

The whole model, discussed in the Introduction, of which a block diagrams representation is shown in Fig. 1, consists of two distinct sections that work alternatively. On the left there is the part for the dynamic simulations to be performed on the considered tracks: the multibody model which interacts online with the global contact model, whereas on the right the part for the evaluation of the wear is shown.

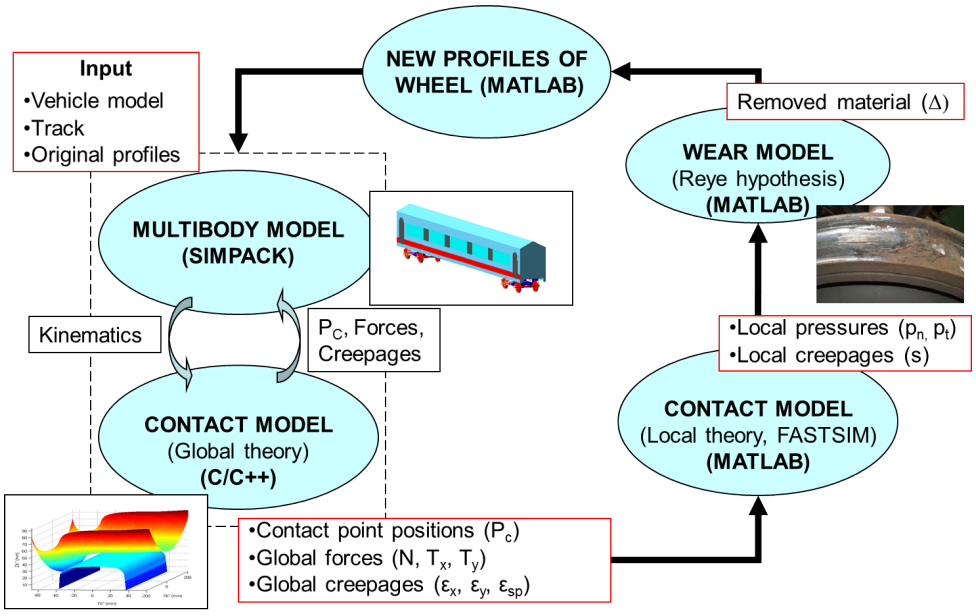

Figure 1: General Architecture of the Model.

During the simulations of each step of the whole procedure, the multibody model implemented in SIMPACK exchanges data continuously at each time step online with the global

contact model, passing the kinematic variables and receiving the positions of the contact points and the wheel-rail contact forces, which are calculated by means of the global contact variables. The wheel profile is the kept constant to the end of the dynamic simulations. Once a simulations step is completed, the local contact model, written in MATLAB and based on the FASTSIM algorithm, is used to evaluated the total friction work done during the travelled distance in each contact patch and its distribution; afterwards, the new wheel profile is evaluated with the wear model using the Reye hypothesis.

The evolution of the wear can be treated in different manners, depending of the type of results expected. If the aim is the analysis of the phenomenon on a complex railway line with many vehicles in service, a statistical approach is necessary to obtain general significant results. In this work, the entire considered railway line has been handled dividing it in a series of a different simulations on curved tracks, classified by radius, superelevation and speed. Therefore, the simulations work is not performed on the real railway line considered, which could be a complex scenery composed by many tracks, eventually very long, where different vehicles are in service; conversely, they are are performed on a equivalent representation of this railway net, derived from statistical methods.

3 The "Minuetto" Multibody Model

The railway vehicle on which this study has been performed is the ALn 501 "Minuetto" (Fig. 2), a passenger transport unit widely used on the Italian railways. It is composed by three coaches and four bogies with two wheelsets each; the external bogies are motorized whereas the two intermediate trailer bogies are of Jacobs type, hence shared between two coaches (Fig. 3). Likewise the most part of passenger vehicles, there are two stage of suspensions. The primary suspensions, which link the axleboxes with the bogie frame, are constituted by Flexicoil springs, made up of two coaxial springs, which mainly provide the vertical stiffness in this vehicle. Instead, the high longitudinal and lateral stiffness that guarantee the stability against the hunting at high speed, are entrusted to a silent block (a Sutuco spring) placed between the axlebox and the longitudinal linking arm connected to the frame. A non linear damper is responsible for the damping of the vertical displacements.

The secondary suspension stage is arranged with the following elements:

- two airsprings for the vertical stiffness (four in the Jacobs bogie), used to guarantee passengers' comfort and a simple automatic regulation of the coaches height with changes in the vertical loads;
- a longitudinal rod, to transmit the traction and braking efforts;
- a torsion bar, to provide the correct rolling stiffness;
- lateral bumpstops;
- lateral dampers;
- vertical dampers;
- anti-yaw dampers.

In addition, the connection between two coaches is made up by a stiffness element and a damper that attenuates the relative lateral and roll motions.

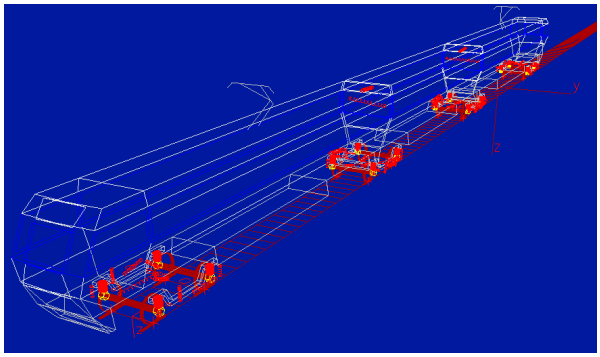

Figure 2: The Aln 501 Minuetto multibody model.

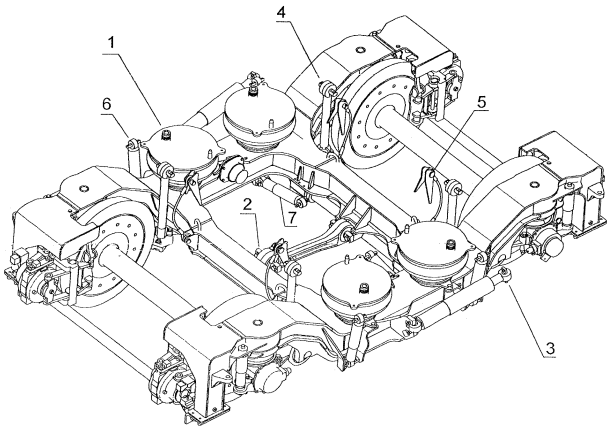

Figure 3: The Jacobs bogie.

The whole SIMPACK multibody model consists of 31 rigid bodies: 3 coaches, 4 bogie frames, 8 wheelsets and 16 axleboxes. The most significant inertial properties inserted in the model are summarized in Tab. 1. The constraints and the force elements are introduced as vis-

	Mass kg	I_{xx} kgm^2	I_{yy} kgm^2	I_{zz} kgm^2	z_G m
External coach	31568	66700	76400	743000	1.91
Internal coach	14496	30600	245000	236000	1.91
Motor bogie frame	3306	1578	2772	4200	/
Trailer bogie frame	3122	1647	3453	5011	/

Table 1: Aln 501 Minuetto main inertial properties.

coelastic force elements, taking into account all the mechanical non linearities where exiting (bumpstops clearances, dampers and rods behavior). In this regard, the main linear characteristics of the suspensions are summarized in Tab. 2; on the contrary, two examples of non linear behavior of dampers in both stage of suspensions are shown in Fig. 4.

Primary suspension	Flexicoil k_z	9.01E+05 N/m
	Flexicoil k_x, k_y	1.26E+06 N/m
	Sutuco k_x	2.0E+07 N/m
	Sutuco k_y	1.5E+07 N/m
Secondary suspension	Airspring k_z	9.01E+05 N/m
	Airspring k_x, k_y	1.2E+05 N/m
	Anti-roll bar k_α	2.6E+06 Nm/rad

Table 2: Main stiffness properties of the ALn 501 Minuetto.

4 The Global Contact Model

The global contact model, used to calculate the contact forces in the wheel-rail interface, exchanges data online with SIMPACK during the multibody simulations at each time step. The latter passes kinematic data to the global contact model, which performs the calculation of the interaction forces. The model is based on a semianalytic approach that guarantees the following features:

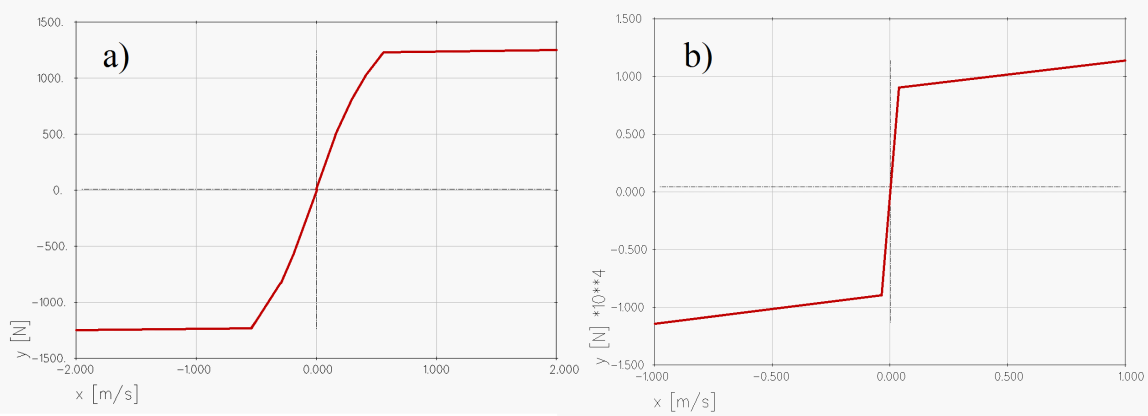

Figure 4: Non linear characteristic of dampers: (a) vertical damper of the primary supension; (b) anti-yaw damper of the secondary suspension stage.

- three-dimensional handling of the problem, with all degrees of freedom between wheel and rail taken into account;
- multiple points of contact with no bounds to the overall number of them;
- performance in terms of computational time and accuracy comparable to other routines included in specialized commercial softwares (Vi-Rail^{TM}, SIMPACK);

The evaluation of these actions consists of two distinct parts: the research of the contact points and the computation of the normal and tangential actions in each contact patch.

4.1 Contact Points Detection

The first task is entrusted to an algorithm developed in previous works (the DIST method [7]) that takes into account the three-dimensionality of the problem and reduces it to a simpler scalar problem, which can be easily handled by means of numerical methods, with the following remarkable advantages:

- the convergence can be easily assured and the algorithm converges to the solutions with a lower number of iterations, and besides, a lower computational effort;
- the management of multiple roots is less difficult;
- a wide range of algorithms, even the elementary non-iterative ones, can be efficiently used to resolve the problem.

The approach is based on the idea that in the contact points, the distance between the wheel surface and rail surface is stationary. The research of these stationary points is equivalent to solve an algebraic system, which can be obtained by imposing geometrical conditions. Fig. 5 shows the nomenclature for the coordinates of a point on the wheel in the two reference systems used to formulate the problem: the *auxiliary system* $O_r x_r y_r z_r$ and the *local system* $O_w x_w y_w z_w$. The first system moves along the centerline of the track following the wheelset; the local system is instead fixed on the wheelset, except for the rotation around the wheelset axle. The DIST method requires that:

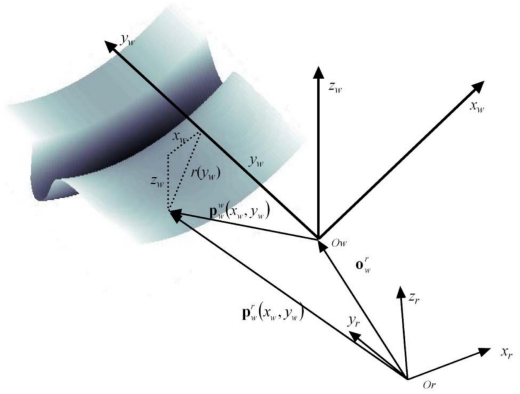

Figure 5: Coordinates of a point on the wheel surface.

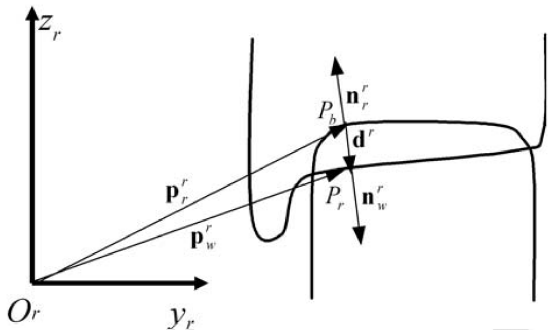

Figure 6: The distance method: vectors involved in the algorithm formulation.

- the normal unitary vector relative to the rail surface $\mathbf{n}_r^r(\mathbf{p}_r^r)$ and the wheel surface unitary vector $\mathbf{n}_w^r(\mathbf{p}_w^r)$ have to be parallel ($\mathbf{R}_2$ is the rotation matrix that links the local system with the auxialiary one):

$$\mathbf{n}_r^r \times \mathbf{n}_w^r(\mathbf{p}_w^r) = \mathbf{n}_r^r(\mathbf{p}_r^r) \times \mathbf{R}_2 \mathbf{n}_w^w(\mathbf{p}_w^w) = \mathbf{0}; \tag{1}$$

- the rail surface normal unitary vector $\mathbf{n}_r^r(\mathbf{p}_r^r)$ has to be parallel to the distance vector $\mathbf{d}^r = \mathbf{p}_w^r - \mathbf{p}_r^r$ between the generic point of the wheel and of the rail:

$$\mathbf{n}_r^r(\mathbf{p}_r^r) \times \mathbf{d}^r = \mathbf{0}. \tag{2}$$

The distance between the generic point of the wheel and of the rail can be written as

$$\mathbf{d}^r(x_w, y_w, x_r, y_r) = \mathbf{p}_w^r(x_w, y_w) - \mathbf{p}_r^r(x_r, y_r) = \mathbf{o}_w^r + \mathbf{R}_2 \mathbf{p}_w^w(x_w, y_w) - \mathbf{p}_r^r(x_r, y_r); \tag{3}$$

so, it depends on four parameters, that identify a point on the wheel and the rail surface. The (1) and (2) constitute a system with six scalar equation and four unknowns (x_w,y_w,x_r,y_r), since only four of the equations are independent. As mentioned previously, the problem can be reduced to two scalar equations in the unknown y_w expressing x_w, x_r, and y_r as functions of y_w. The second component in (1) leads to

$$r_{13}\sqrt{r(y_w)^2 - x_w^2} = r_{11}x_w - r_{12}r(y_w)r'(y_w) \tag{4}$$

where r_{13}, r_{11} and r_{12} are elements of the $\mathbf{R}_2$ matrix. Let $A = r_{13}$, $B = r(y_w)$, $C = r_{11}$ and $D = r_{12}r(y_w)r'(y_w)$; the previous equation becomes

$$A\sqrt{B^2 - x_w^2} = Cx_w - D. \tag{5}$$

Hence, removing the radical and solving for x_w:

$$x_{w1,2}(y_w) = \frac{CD \pm \sqrt{C^2D^2 - (C^2 + A^2)(D^2 - A^2B^2)}}{C^2 + A^2}; \tag{6}$$

therefore, there are two possible values for x_w. In addition, substituting $x_{w1,2}(y_w)$ in first component of (1), the following expression, for the rail profile derivative, can be obtained:

$$b'(y_r)_{1,2} = \frac{r_{21}x_{w1,2}(y_w) - r_{22}r(y_w)r'(y_w) - r_{23}\sqrt{r(y_w)^2 - x_{w1,2}(y_w)^2}}{r_{32}r(y_w)r'(y_w) + r_{33}\sqrt{r(y_w)^2 - x_{w1,2}(y_w)^2}} \tag{7}$$

Considering separately both sides of the track, if $b'(y_r)_{1,2}$ is a decreasing monotonous, the (7) is numerically invertible, that will give $y_{r1,2}$; otherwise, the inversion is possible anyway and will produce a further multiplication of the solution number. Furthermore, the second scalar component of (2) can be rewritten as

$$x_{r1,2}(y_w) = r_{11}x_{w1,2}(y_w) + r_{12}y_w - r_{13}\sqrt{r(y_w)^2 - x_{r1,2}(y_w)^2}. \tag{8}$$

The values of the three variables x_w, x_r and y_r can now be inserted in the first component of the (2), to write the following relation:

$$\begin{aligned} F_{1,2}(y_w) = -b'(y_{r1,2}(y_w))\Big(G_z + r_{32}y_w - r_{33}\sqrt{r(y_w)^2 - x_{w1,2}(y_w)^2} - b\big(y_{r1,2}(y_w)\big)\Big) \\ - \Big(G_y + r_{21}x_{w1,2}(y_w) + r_{22}y_w - r_{23}\sqrt{r(y_w)^2 - x_{w1,2}(y_w)^2} - y_{r1,2}(y_w)\Big) = 0; \end{aligned} \tag{9}$$

the (9) are two simple scalar equations in the y_w variable, easy to resolve numerically with the advantages previously mentioned; let y^C_{w1j} be the solution of $F_1(y_w)$ and y^C_{w2k} the root of $F_2(y_w)$. The dimension of the initial problem has been reduced from 4 to 1, as discussed above.

Since the equation includes irrational terms, a root can be accepted only if it satisfies all the following conditions:

- x^C_{w1j} and x^C_{w2k} (calculated by (6) for y^C_{w1j}, y^C_{w2k}) have to be real numbers;
- the terms $\sqrt{r(y^C_{w1j})^2 - x(y^C_{w1j})^2}$ and $\sqrt{r(y^C_{w2k})^2 - x(y^C_{w2k})^2}$ of (9) have to be real too;
- (x^C_{w1j}, y^C_{w1j}) and (x^C_{w2k}, y^C_{w2k}) have to be effective solutions of (4);
- the penetration between the wheel and rail surfaces ($p_n = \mathbf{d}^r \cdot \mathbf{n}^r_r$) have to be less or equal to zero;
- the root is not a multiple solution;
- the normal curvatures of the wheel and rail surfaces in the longitudinal and lateral direction ($k_{1,wi}$, $k_{1,ri}$, $k_{2,ri}$, $k_{2,ri}$) have to allow the contact in that point ($k^C_{1,wi} + k^C_{1,ri} > 0$; $k^C_{2,wi} + k^C_{2,ri} > 0$).

4.2 Evaluation of the contact forces

The calculation of the contact forces is based on a semi-elastic approach which uses the theories of Hertz and Kalker. The normal contact forces, according to the Hertz theory, depend both on the penetration (p_n) between the surface of the wheel and rail and the penetration velocity v_n:

$$N^b(\mathbf{p}^{b,C}_b) = \left[- k_h|p_n|^\gamma + k_v|v_n|\frac{\mathrm{sgn}(v_n) - 1}{2}\right]\frac{\mathrm{sgn}(p_n) - 1}{2} \tag{10}$$

where γ is equal to 3/2, k_h is a Kalker's stiffness costant, k_v is a damping contact constant [4]. The application of the same theory leads to the evaluation of the contact patches semiaxis and

eccentricity. The linear Kalker's theory is used to calculate the tangential forces and the spin moment (Fig. 7) in each contact patch:

$$T_x^b(\mathbf{p}_b^{b,C}) = -f_{11}\xi_x \tag{11}$$
$$T_y^b(\mathbf{p}_b^{b,C}) = -f_{22}\xi_y - f_{23}\xi_{sp} \tag{12}$$
$$M_{sp}^b(\mathbf{p}_b^{b,C}) = -f_{23}\xi_y - f_{33}\xi_{sp} \tag{13}$$

where the value of the f_{ij} coefficients, which are function of the material properties and the ellipse semiaxis, can be found in literature [4]; ξ_x, ξ_y and ξ_{sp} are the longitudinal, lateral and the spin creepages, as defined below:

$$\xi_x = \mathbf{v}\cdot\mathbf{i}_b \Big/ \left\|\dot{G}_{w,f}^b\right\|; \qquad \xi_y = \mathbf{v}\cdot\mathbf{t}_b^b \Big/ \left\|\dot{G}_{w,f}^b\right\|; \qquad \xi_{sp} = \boldsymbol{\omega}^b\cdot\mathbf{n}_b^b \Big/ \left\|\dot{G}_{w,f}^b\right\| \tag{14}$$

where $\dot{G}_{w,f}^b$ is the absolute velocity of the wheelset centre of mass.

Since the Kalker's theory is linear, a saturation criterion is introduced to reproduce the existence of an adhesion limit due to friction: indeed, the magnitude of the tangential contact force $\|\tilde{\mathbf{T}}^b\| = \sqrt{\tilde{T}_x^{b2} + \tilde{T}_y^{b2}}$ cannot exceed the slip value $T_s^b = \mu N^b$. Therefore, a saturation coefficient ϵ [15] is introduced, such that $\mathbf{T}^b = \epsilon\tilde{\mathbf{T}}^b$, where $\mathbf{T}^b$ is the effective tangential force vector.

$$\epsilon = \begin{cases} \dfrac{\mu N^b}{\tilde{T}^b}\left[\left(\dfrac{\tilde{T}^b}{\mu N^b}\right) - \dfrac{1}{3}\left(\dfrac{\tilde{T}^b}{\mu N^b}\right)^2 + \dfrac{1}{27}\left(\dfrac{\tilde{T}^b}{\mu N^b}\right)^3\right] & \text{if } \tilde{T}^b \le 3\mu N^b \\ \dfrac{\mu N^b}{\tilde{T}^b} & \text{if } \tilde{T}^b > 3\mu N^b \end{cases} \tag{15}$$

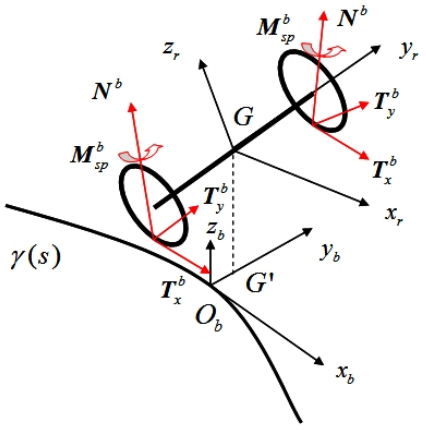

Figure 7: Nomenclature of the contact forces.

5 The local contact model

Once the multibody simulations have been carried out on all the curves included in the statistical analysis, the local contact model performs the calculation of the local contact variables (normal pressures, tangential stresses and creepages) within each contact patch, starting from

the global contact variables (contact points position, contact forces and spin moments, creepages and patch semiaxis). The model utilizes an approximate but very efficient version of the Kalker's local theory implemented in his FASTSIM algorithm, widely used in railway applications [4].

The fundamental hypothesis of the algorithm is the proportionality between the tangential pressure $\mathbf{p}_t$ and the elastic displacements $\mathbf{u}$ in a generic point of the contact patch:

$$\mathbf{u}(x,y) = L\mathbf{p}_t(x,y); \qquad L = L(\boldsymbol{\epsilon}, a, b, G, \nu) \tag{16}$$

where the flexibility L is a function of the rigid creepage vector $\boldsymbol{\epsilon}$, the ellipse semiaxes a, b, the combined shear modulus G and the combined Poisson's coefficient ν [4].

On the contrary, the local creepage $\mathbf{s}$ can be calculate deriving the elastic displacements and taking into account the rigid creepages and the vehicle speed V:

$$\mathbf{s}(x,y) = \dot{\mathbf{u}}(x,y) + V\left[\epsilon_x \;\; \epsilon_y\right]^T. \tag{17}$$

The local variables p_n, $\mathbf{p}_t$ and $\mathbf{s}$ are calculated in each point of a grid that discretizes the contact patch (Fig. 8) with a non constant longitudinal resolution Δx to improve the accuracy near the edges.

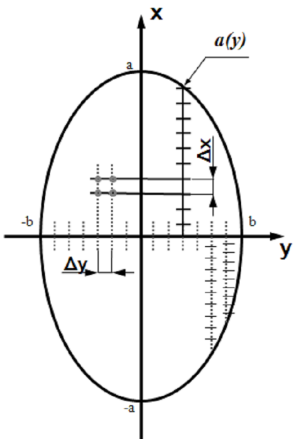

Figure 8: Contact patch discretization in the FASTSIM algorithm.

The FASTSIM algorithm allows to evaluate iteratively the values of p_n, $\mathbf{p_t}$ as well as the local slip $\mathbf{s}$ in the contact patch. Let (x_i, y_i) $1 \leq i \leq n_x$, $1 \leq j \leq n_y$ be the generic point of the contact patch grid (typical values for n_x, n_y are $25 \div 50$); hence the normal pressure and the adhesion limit pressure $\mathbf{p}_A$ can be expressed as follows:

$$p_n(x_i, y_j) = \frac{3}{2}\frac{N}{\pi ab}\sqrt{1 - \frac{x_i^2}{a^2} - \frac{y_j^2}{b^2}} \tag{18}$$

$$\mathbf{p_A}(x_i, y_j) = \mathbf{p_t}(x_{i-1}, y_j) - \begin{bmatrix} \epsilon_x \\ \epsilon_y \end{bmatrix}\frac{\Delta x(y_j)}{L} = \mathbf{p_t}(x_i - \Delta x(y_j), y_j) - \begin{bmatrix} \epsilon_x \\ \epsilon_y \end{bmatrix}\frac{\Delta x(y_j)}{L} \tag{19}$$

where N is the normal contact force. The iterative formulation of the algorithm is the following:

$$\|\mathbf{p_A}(x_i, y_j)\| \;\leq\; \mu p_n(x_i, y_j) \Rightarrow \mathbf{p_t}(x_i, y_j) = \mathbf{p_A}(x_i, y_j); \quad \mathbf{s}(x_i, y_j) = \mathbf{0} \tag{20}$$

$$\|\mathbf{p_A}(x_i, y_j)\| \;>\; \mu p_n(x_i, y_j) \Rightarrow \begin{cases} \mathbf{p_t}(x_i, y_j) = \mu p_n(x_i, y_j)\mathbf{p_A}(x_i, y_j)/\|\mathbf{p_A}(x_i, y_j)\| \\ \mathbf{s}(x_i, y_j) = \frac{LV}{\Delta x(y_j)}\big(\mathbf{p_t}(x_i, y_j) - \mathbf{p_A}(x_i, y_j)\big) \end{cases} \tag{21}$$

Assuming the boundary conditions $\mathbf{p_t}(x_1, y_j) = \mathbf{0}$, $\mathbf{s}(x_1, y_j) = \mathbf{0}$, $1 \leq j \leq n_y$ (the creepages and the pressures have to be zero out of the contact patch), the distributions of the pressures $p_n(x_i, y_j)$, $\mathbf{p_t}(x_i, y_j)$ and the creepages $\mathbf{s}(x_i, y_j)$ are obtained iterating the procedure for $2 \leq i \leq n_x$ and $1 \leq j \leq n_y$.

6 The Wear Model

6.1 The Reye Hypothesis

The approach to the analysis of the wear has been developed on the basis of the following hypothesis:

- only the wheels are subject to wear, whereas the rail profiles are constant and new;
- the only wear mechanism taken into account is the abrasion;
- dry conditions in the wheel-rail interface;

The distribution of the wear on the wheel is based on a three-dimensional variant of the Reye hypothesis which asserts that the volume of removed material is proportional to the total work done by the friction forces:

$$\delta V = C \delta L_F.$$

The variant implemented in the wear model allows to estimate the thickness $\delta_{P_{wi}^{jk}}(t)$ (in mm), that is a function of the time which describes the height of removed material from the wheel $j\text{-}th$ ($1 \leq j \leq N_W$) due to the wear in the contact patch $i\text{-}th$ ($1 \leq i \leq N_P$) in the $k\text{-}th$ multibody simulation of the statistical analysis ($1 \leq k \leq N_C$) (which will be explained in the next paragraph). The estimation of $\delta_{P_{wi}^{jk}}(t)$ needs the evaluation of the frictional power produced by the tangential contact pressures, with which a *wear index* I_W (N/mm^2) can be defined:

$$I_W = \frac{\mathbf{p_t} \cdot \mathbf{s}}{V}, \tag{22}$$

where $\mathbf{s}$ is the local absolute creepage. By analyzing experimental results, this index can be related with the wear rate K (μg/m·mm^2), the amount of removed material per metre of traveled distance (m) covered by the train and per mm^2 of surface. The cases of a steel-steel contact under dry conditions are available in literature, for example in [10], [12].

The experimental relationship between $K(I_W)$ used in the model is shown in Fig. 9 next to the analytic description. Once $K(I_W)$ is known, the depth of removed material $\delta_{P_{wi}^{jk}}(x, y)$ can be calculated as follows:

$$\delta_{P_{wi}^{jk}(t)}(x, y) = K(I_W) \frac{V \Delta t}{\rho} \frac{V \Delta t}{2\pi R(y_{wi})}; \tag{23}$$

in which ρ is the material density (expressed in kg/m^3), $R(y_{wi})$ is the wheel radius in the y_{wi} point and Δt is the discrete integration time step. The factor $V\Delta t/\rho$ allows to obtain, multiplying by $K(I_W)$, the depth of removed material locally, whereas the adimensional factor $V\Delta t/(2\pi R(y_{wi}))$ acts as an average along the wheel circumference, providing the actual depth of removed material.

Since there are other wear mechanisms that the model does not take into account besides the abrasion, it has to be tune properly to do not underestimate the global wear rate. The tuning

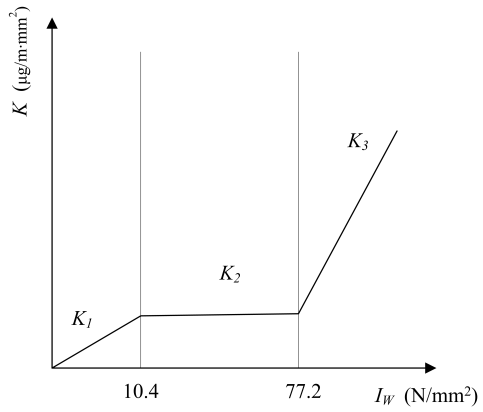

$$K_W(I_W) = \begin{cases} 5.3 \cdot I_W & I_W < 10.4 \text{ N/mm}^2 \\ 55.0 & 10.4 \leq I_W \leq 77.2 \text{ N/mm}^2 \\ 61.9 \cdot I_W & I_W > 77.2 \text{ N/mm}^2 \end{cases}$$

Figure 9: Wear rate for different values of the wear index.

is based on the minimization of the error in the comparison between numerical results and experimental data, relating to the Aosta-Pre Saint Didier line, has been performed acting on the parameters of the filter used to smooth the wheel profile arising from the material removal. Thus, the filter has a double purpose:

- it allows to introduce the effect of other wear contributions neglected (i.e. the plasticity wear, mainly);
- it eases the noise in the distribution of the material to be removed, cutting the short wavelengths in the wheel profile that lead up to problems in the global contact model.

6.2 The Profile Update

A critical step in the general loop of the wear model is the profile update, that is the whole of the numerical procedures that leading to the new wheel profile $r_n(y_w)$ (to be used in the next step) starting from the knowledge of previous wheel profile $r_p(y_w)$ (at the current step) and the distribution of the removed material $\delta_{P^{jk}_{wi}}(x, y)$. These procedures arise from the following distinct issues:

- the distribution $\delta_{P^{jk}_{wi}}(x, y)$ is characterized by a remarkable numerical noise and if no numerical treatments were applied, the new wheel profile would not be physical because of the presence of short spatial wavelengths as well as it would lead to serious contact problem;
- the distribution $\delta_{P^{jk}_{wi}}(x, y)$ does not consider other important wear mechanisms;
- the output of the wear model has to be a single wheel profile: the numerical treatment and the removal of material are not carried out on each wheel separately.

The main phases of the update are described below:

1) Longitudinal integration:

$$\int_{-a(y)}^{a(y)} \delta_{P^{jk}_{wi}}(x, y)dx = \delta_{P^{jk}_{wi(t)}}(y); \tag{24}$$

The aim of this operation is the sum of all wear contributions in the longitudinal direction along the contact patch.

2) Time integration:

$$\int_{T_i}^{T_f} \delta_{P_{wi}^{jk}}(s_w - s_{wi}^C(t))dt = \Delta_{P_{wi}^{jk}}(s_w); \tag{25}$$

since $y \cong s_w - s_w^C$; s_w is the generic curvilinear abscissa and $s_w^C(t)$ the curvilinear abscissa of the contact point on the wheel at the time t. This integration performs the sum of all the contributions during the simulation.

3) Sum on the contact points:

$$\sum_{i=1}^{N_P} \Delta_{P_{wi}^{jk}}(s_w) = \Delta_{jk}(s_w); \tag{26}$$

where N_P is the maximum number of the possible contact points on a single wheel (since the number of these points is usually less than N_P and not constant over the time, the contribution to the wear of the fictitious points is set equal to zero); in addition, the quantity $\Delta_{jk}(y_w)$ is the removed material of the $j\text{-}th$ wheel during the $k\text{-}th$ dynamic simulation.

4) Average on the wheels and the simulations:

$$\sum_{i=1}^{N_C} p_k \frac{1}{N_W} \sum_{j=1}^{N_W} \Delta_{jk}(s_w) = \bar{\Delta}(s_w); \tag{27}$$

where N_W is the number of the vehicle wheels while p_k, $1 \leq k \leq N_C$, $\sum_{i=1}^{N_C} p_k = 1$ are the weights related to the dynamic simulations; the average on the vehicle wheels is done to have a single mean profile as output, whereas the introduction of the weights p_k allows to take into account the different statistical influence of each curve of the whole N_C.

5) Scaling:

$$\bar{\Delta}(s_w)\frac{km_{step}}{km_{runs}} = \bar{\Delta}^{sc}(s_w); \tag{28}$$

The amount of removed material $\bar{\Delta}(s_w)$ is related to the overall mileage traveled by the vehicle during the N_C simulations performed along the discrete step chosen, that is $km_{runs} = N_C L_C$, (where L_C is the length of curved tracks on the which the vehicle dynamics has been simulated). However, this mileage could be quite shorter than the overall mileage km_{tot} that the vehicle has to run, hence, to complete the total distance, an excessive number of discrete steps may be necessary, with a significant increase in the computational time. The linearity of the wear model can help overcome the problem by scaling conveniently the amount of removed material $\bar{\Delta}(s_w)$ (Eq. 28). The scaled quantity of material $\bar{\Delta}^{sc}(s_w)$ is now related to a spatial step with a length equal to km_{step}, with which the km_{tot} is discretized.

Nevertheless, the choice of the spatial step has to be done as a compromise between numerical efficiency and accuracy required by the wear model. A short km_{step} respect to the km_{tot} leads to an accurate approach to the phenomenon, requiring high computational efforts; the vice versa occurs choosing an excessive km_{step}. The km_{step} can be variable and controlled by means of an adaptive procedure; for example, updating it, by imposing that the amount

of removed material $\bar{\Delta}^{sc}(s_w)$ cannot overcome an establish threshold, or simply constant and sufficiently shorter than km_{tot}.

For the validation with the experimental data of the Aosta-Pre Saint Didier line, 3500 km long, the two strategies have given comparable results (mainly for the regular evolution of the profile with the increasing of the traveled distance). Therefore, a constant km_{step} equal to 350 km has been chosen, since this strategy is more efficient numerically.

6) Smoothing of the amount of removed material:

$$\Im\left[\bar{\Delta}^{sc}(s_w)\right] = \bar{\Delta}^{sc}_{sm}(s_w); \tag{29}$$

the smoothing for this distribution is necessary to filter the numerical noise which characterizes this quantity, avoiding its transfer to the new wheel profile $r_n(y_w)$ and the resulting problems for the global contact model. A first order discrete filter has been used [13], that is a sliding mean with a window width equal to the $1\% \div 5\%$ of the total points that discretize the wheel profile. Clearly, other filters could be used, provided that the total mass of removed material will remain unchanged.

7) Profile update:

$$\begin{pmatrix} y(s) \\ r_p(s) \end{pmatrix} + \bar{\Delta}^{s}_{sm}(s_w)\underline{n}^{r}_{r} \xrightarrow{re-parametrization} \begin{pmatrix} s^* \\ r_n(s^*) \end{pmatrix} \tag{30}$$

The last phase consists in the updating of the previous profile $r_p(y_w)$ to obtain the new profile $r_n(y_w)$ for the next step; the material is removed in the normal direction to the profile. Once the quantity $\Delta^{sc}_{sm}(s_w)$ is subtracted, a new parametrization has to be carried out to make the wheel profile an explicit function of the variable y_w.

7 Validation of the Model

Before discussing the results of the validation, a brief introduction to the railway line, the parameters involved and the experimental data with their treatment will be presented in this paragraph.

7.1 The Aosta-Pre Saint Didier line

As mentioned in the Introduction, a statistical approach has been chosen to arrange the total simulation work, avoiding the treatment of the entire railway line which would lead to excessive long simulations. Thus, an equivalent description of the line has been derived analyzing the whole database of the Aosta-Pre Saint Didier line provided by Rete Ferroviaria Italiana; the whole track has been converted in a representative series of curved tracks with different radius and superelevation, reducing the overall mileage to be simulated. The wear is evaluated along each of all curves, neglecting the contributions of the transition lengths, which cannot be considered in this approach. The procedure may be particularly useful to simplify the investigation of the wear in a complex railway line composed by many tracks.

The statistical approach to the Aosta-Pre Saint Didier railway line has led to the classification shown in Fig. 10, composed by N_C different classes (17 curves and the straight part); as visible in the four last columns, each of them is characterized by a curve radius R_C, a superelevation h, a traveling speed V and a percentage weight p_k, $1 \leq k \leq N_C$, which represents the frequency of a class, that has to be taken into account in the wear evaluation. Blank rows are present because

for each mean radius curve only one or two superelevation in the range $0 \div 160$ mm (column 2) have been considered. In addition, since the track is very winding, the speed range is narrow and the max speed is quite low (70 km/h).

The wheel-rail coupling in this scenery is characterized by the ORE S1002 wheel profile, the UIC60 rail profile and the 1:20 rad rail inclination.

Min. radius (m)	Max. radius (m)	Superelevation range (mm)	Mean radius (m)	Rounded radius (m)	h (mm)	V (km/h)	%
147.0588	156.25	0	0.0				
		10 A 40	0.0				
		60-80	0.0				
		90-120	150.0	150	120	55	0.77%
		130-160	0.0				
156.3	166.7	0	0.0				
		10 A 40	0.0				
		60-80	0.0				
		90-120	162.6	160	110	55	0.48%
		130-160	164.0	165	140	55	0.56%
166.7	178.6	0	0.0				
		10 A 40	0.0				
		60-80	0.0				
		90-120	169.6	170	110	55	0.82%
		130-160	173.1	175	130	55	1.55%
178.6	192.3	0	0.0				
		10 A 40	0.0				
		60-80	0.0				
		90-120	187.9	190	100	55	8.37%
		130-160	180.1	180	130	55	0.45%
192.3	208.3	0	0.0				
		10 A 40	0.0				
		60-80	0.0				
		90-120	198.6	200	90	55	20.64%
		130-160	197.6	200	130	60	4.00%
208.3	227.3	0	0.0				
		10 A 40	0.0				
		60-80	219.8	220	80	55	0.70%
		90-120	218.6	220	100	55	3.76%
		130-160	0.0				
227.3	250.0	0	0.0				
		10 A 40	0.0				
		60-80	240.8	240	80	55	7.26%
		90-120	240.9	240	110	60	5.28%
		130-160	0.0				
250.0	312.5	0	0.0				
		10 A 40	0.0				
		60-80	267.9	270	70	55	3.91%
		90-120	270.2	270	90	60	5.29%
		130-160	0.0				
312.5	416.7	0	0.0				
		10 A 40	0.0				
		60-80	369.4	370	60	55	2.26%
		90-120	345.5	345	100	70	1.63%
		130-160	0.0				

Figure 10: The N_C tracks arising from the statistical analysis.

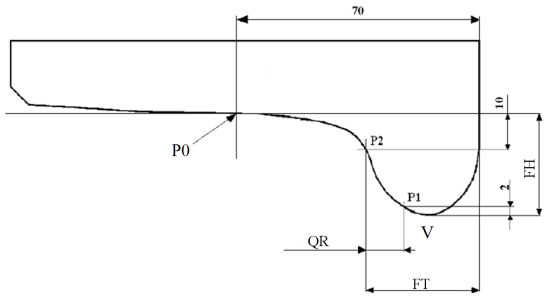

Figure 11: Reference dimensions of the wheel profile.

7.2 Reference dimensions

To estimate the wear of a wheel profile, three reference dimensions (flange thickness FT, flange height FH, QR dimension, Fig. 11) can be measured avoiding a complete detection of its geometry. The evolution of these parameters allows to decide whether the profile has to be returned or not, considering both the running stability conditions and the maximum or minimum allowable values of these dimensions before the end of life of the wheel, and consequently, of the wheelset.

The three dimensions are defined in the following manner:

- first of all, the point P0, 70 mm distant from the internal side of the wheel is identified on the profile;

- the point P1 on the profile is introduced 2 mm below from the lowest point V of the flange;
- the point P2 is identified 10 mm below from P0;
- the flange thickness SP is the distance between P2 and internal vertical side of the wheel; QR is the vertical distance between P1 and P0; finally, the flange height FH is the vertical distance between P0 and V.

From a physical viewpoint, both the flange thickness FT and the flange height FH describe the size of the flange, while the flange height is also a measure of the wear on the wheel tread; QR gives information about the conicity instead. Moreover, the adopted dimensions do not depend on the wheel rolling radius.

7.3 Treatment of the experimental data

The available experimental data relative to the Aosta-Pre Saint Didier include the evolution of the three dimensions above discussed (FT, FH, QR) as a function of the distance traveled by the ALn 501 "Minuetto". The measured dimensions were taken on three different vehicle operating on the same line, which are conventionally named MD061, MD068, MD082. Fig. 12 shows the dimensions of the MD061 vehicle as example.

km	flange dimensions	1 r	1 l	2 r	2 l	3 r	3 l	4 r	4 l	5 r	5 l	6 r	6 l	7 r	7 l	8 r	8 l
		wheel radius 816 mm		wheel radius 815 mm		wheel radius 824 mm		wheel radius 823 mm		wheel radius 823 mm		wheel radius 823 mm		wheel radius 819 mm		wheel radius 820 mm	
0	FT	30.953	30.944	30.983	30.784	31.099	30.957	30.938	31.076	30.401	30.367	30.830	30.987	30.437	30.717	30.852	30.933
	FH	27.970	27.894	28.141	28.043	27.969	28.187	28.030	28.271	28.245	27.918	28.141	27.982	28.013	27.937	28.333	27.883
	QR	10.208	10.140	10.424	10.457	10.220	10.306	10.279	10.833	10.332	10.445	10.364	10.219	10.421	10.500	10.338	10.396
1426	FT	29.855	28.977	30.283	29.317	30.118	29.383	30.152	29.450	29.796	29.799	30.288	29.483	29.802	29.085	30.267	29.316
	FH	28.010	27.923	28.104	28.108	28.000	28.249	28.095	28.278	28.248	28.284	28.247	28.030	28.997	28.003	30.383	27.919
	QR	9.297	8.226	9.822	8.956	9.344	8.749	9.511	9.072	9.635	9.767	9.773	8.763	9.593	8.883	9.675	8.762
2001	FT	29.056	28.498	29.722	28.878	29.441	28.667	29.629	28.717	29.153	28.101	29.739	28.841	29.066	28.447	29.625	28.777
	FH	27.990	27.880	28.161	28,0,80	29.998	28.248	28.128	28.283	28.290	27.994	28.273	28.022	28.027	28.014	28.362	27.957
	QR	8.404	7.558	9.233	8.637	8.702	7.950	8.873	8.436	9.144	8.141	9.236	8.086	9.038	8.152	9.248	8.373
2575	FT	28.259	27.096	29.333	28.045	28.972	28.385	29.029	28.124	29.053	27.600	29.095	28.505	28.553	27.866	29.205	28.473
	FH	28.009	27.089	28.173	28.020	28.063	28.243	28.090	28.241	28.285	27.963	28.244	28.085	28.030	28.018	28.352	27.968
	QR	7.198	7.024	8.853	8.163	8.123	7.598	8.438	7.791	8.868	7.395	8.559	7.840	8.372	7.340	8.777	7.900

Figure 12: Experimental data of the ALn 501 "Minuetto" MD061.

Since the reference dimensions were measured on all the sixteen wheels of each vehicle, a data processing has been performed taking the average on the whole of them to extrapolate an unique progress for every vehicle as shown in Tab. 3, in order to make possible a comparison with the wheel profile arising from the numerical simulations. The steps are the following:

- scaling of the dimensions to eliminate the initial offsets, imposing that all the quantities have the nominal value at the beginning of the mileage;
- average of each dimensions on the sixteen wheels of a vehicle, to establish an unique wheel profile progress for comparisons with the numerical results.

As visibile in Tab. 3, the average has been performed obtaining a profile for each "Minuetto" (MD061, MD068, MD082) without a further average on the three vehicles to preserve the behavior of each of them, thus guaranteeing a tolerance zone for a better and more significant fitting with the experimental data.

Vehicle	km	QR	FH	FT
MD061	0	10.8	28.0	32.5
	1426	9.8	28.2	31.5
	2001	9.1	28.1	30.8
	2575	8.6	28.0	30.2
MD068	0	10.8	28.0	32.5
	1050	10.0	28.0	31.8
	2253	8.5	28.0	30.2
	2576	8.4	28.0	32.5
MD082	0	10.8	28.0	32.5
	852	10.6	28.0	32.3
	1800	9.6	28.0	31.3
	2802	8.7	28.8	30.3
	3537	8.3	27.6	30.0

Table 3: Averaging and scaling of experimental data

7.4 Progress of the reference dimensions

In this section, the progress of the three dimensions (flange thickness FT, flange height FH and QR dimension) numerically evaluated with the wear model will be compared with the experimental values of the three vehicles. The filter parameters (width of the window and number of applications) have been chosen to minimize the error respect to the experimental data.

The progress of the FT dimension is shown in Fig. 13 as a function of the mileage; as it can be seen, the decrease of the dimension is almost linear with the traveled distance except in the first phases, where the profiles are not conformal enough. The FH curve is presented in Fig. 14, which shows that, due to the presence of many sharp curves in the track, the wear is localized mainly on the flange instead of the tread, while the flange height remains nearly constant.

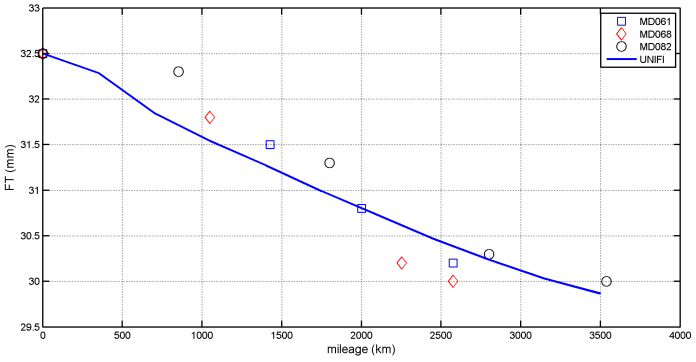

Figure 13: FT dimension progress.

Finally, the QR trend is shown in Fig. 15: the dimension decreases almost linearly too, leading to an augment of the equivalent conicity in the wheel-rail coupling. Although the simulated mileage is quite short taking into consideration the mean traveled distance between two turning of wheels in a similar scenery, the variation of the FH and QR dimensions is remarkable and it evidences difficulties in terms of wear in the circulation along the railway line.

As a conclusion, the comparisons show that the outputs of the wear model are very consistent with the experimental data, both for the flange dimensions and the conicity (QR); hence, the validation of the model can be considered satisfactory.

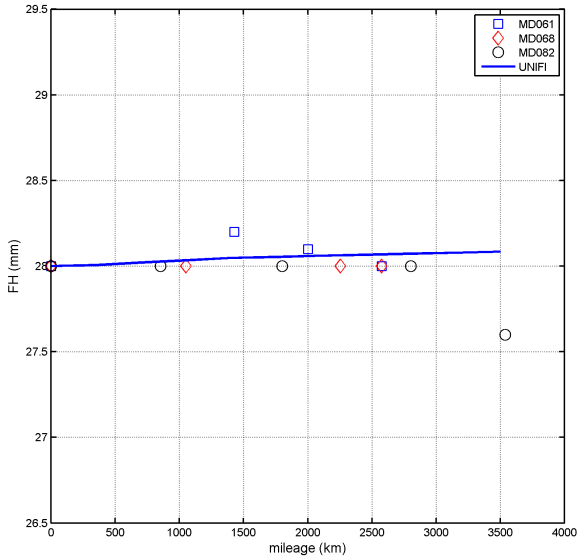

Figure 14: FH dimension progress.

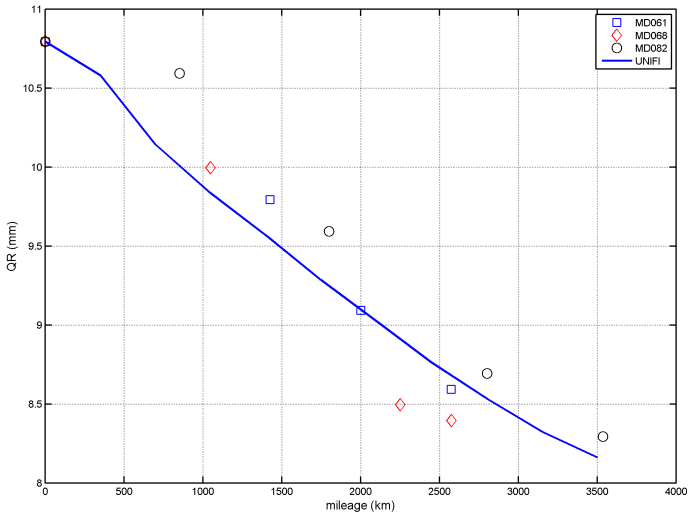

Figure 15: QR dimension progress.

7.5 Progress of the wheel profile

The evolution of the wheel profile, calculated with the wear model, is presented in Fig. 16. As stated previously, it is described by means of 10 steps, since the total distance km_{tot} is 3500 km and the spatial step km_{step} has been chosen equal to 350 km. The effect of wear on the tread is rather low and entails a slight reduction of the rolling radius. However, observing the flange zone, the wear rate is higher during the first steps because of the non-conformal contact due to the coupling between the ORE S1002 profile and the UIC60 rail with a inclination of 1:20 rad; then it decreases becoming more regular and constant in the last phases, when the contact is more and more conformal. The situation is clarified with the enlargement of the flange zone, shown in Fig. 17: the distance between two profiles drops off as the wear increases.

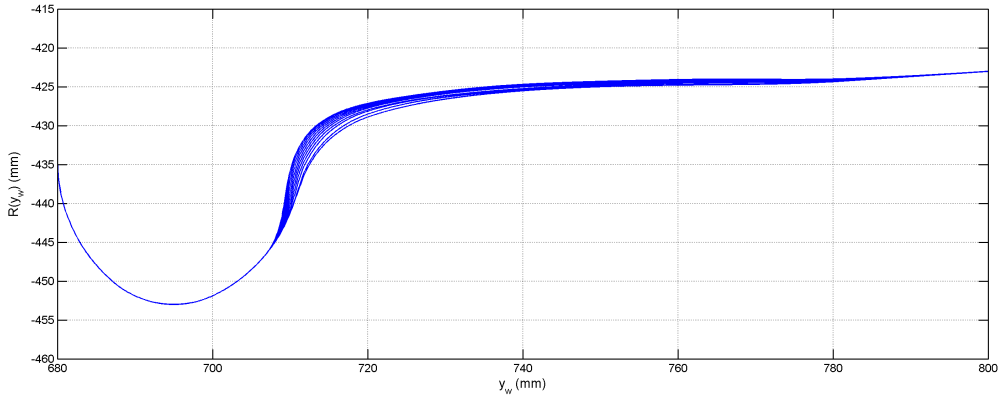

Figure 16: Evolution of the wheel profile.

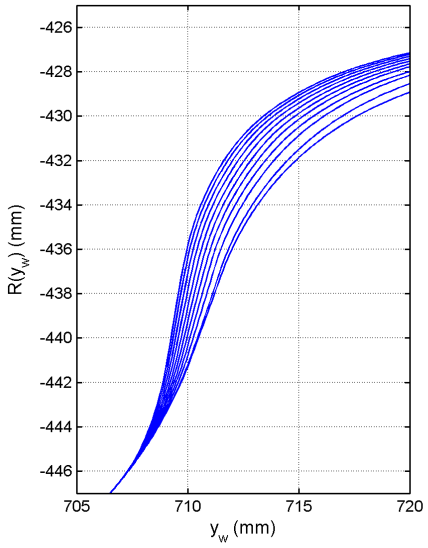

Figure 17: Evolution of the profile in the flange zone.

8 Conclusions

In this work the Authors have presented a complete model for the wheel wear prediction in railway applications, developed thanks to the collaboration with Trenitalia S.p.A and Rete Ferroviaria Italiana, which provided the necessary technical and experimental data. The whole structure is mainly composed by two parts which mutually interact: the first one is the vehicle dynamics which comprises both the multibody model implemented with SIMPACK and a global wheel-rail contact model for the contact force calculations; the second one is the wear model, which uses the output of multibody simulations to evaluate the amount of material to be removed due to wear. The interaction between the two subsystems is not a continuous time process but occurs in discrete steps, so the evolution of the wheel geometry during the overall mileage is described through several intermediate profiles.

The entire model has been validated exploiting the experimental data relative to a particularly critical scenery in terms of wear in the Italian railways: the ALSTOM Aln 501 “Minuetto” circulating on the Aosta-Pre Saint Didier railway line. A statistical approach to describe the track has been used to reduce the total computational effort. The arising model reproduces

properly the evolution of all the three characteristic dimensions of the wheel profile which describe the wear progress. The resultant wheel profile evolution demonstrates how, in this particular application, the wear is severe and strongly localized on the flange of wheel, leading to frequent maintenance interventions.

Future developments may consist in the evaluation of the rail wear evolution and the implementation of other wear mechanisms.

9 ACKNOWLEDGEMENTS

Authors would like to thank Engg. R. Cheli and G. Grande of Trenitalia S.p.A for providing and giving the permission to edit the data relative both to the vehicle ALn 501 Minuetto and to the wheel wear evolution; a special thanks also goes to the Engg. R. Mele and M. Finocchi of Rete Ferroviaria Italiana for the data relative to the Aosta-Pre Saint Didier line.

REFERENCES

[1] A. A. Shabana, J. R. Sany. An augmented formulation for mechanical systems with non-generalized coordinates: application to rigid body contact problems. *Nonlinear Dynamics*, **24**, 183–204, 2001.

[2] S. Iwinicki. Simulation of wheel - rail contact forces. *Fatigue and Fracture of Engineering Materials and Structures*, **26**, 887–900, 2003.

[3] J. Pombo, J. Ambrosio. Dynamic analysis of a railway vehicle in real operation conditions using a new wheel - rail contact detection model. *International Journal of Vehicle Systems Modelling and Testing*, **1**, 79–105, 2005.

[4] J. J. Kalker. *Three - dimensional Elastic Bodies in Rolling Contact*. Kluwer Academic Publisher, Dordrecht, 1990.

[5] R. V. Dukkipati, J. R. Amyot. *Computer Aided Simulation in Railway Dynamics*. Dekker, New York, 1988.

[6] A. A. Shabana, K. E. Zaazaa, J. L. Escalona and J. L. Sany. Development of elastic force model for wheel/rail contact problems. *Journal of Sound and Vibration*, **269**, 295–325, 2004.

[7] E. Meli, S. Falomi, M. Malvezzi and A. Rindi. Determination of wheel - rail contact points with semianalytic methods. *Multibody System Dynamics*, **20(4)**, 327–358, 2008.

[8] S. Iwinicki. *The Manchester Benchmarks for Rail Vehicle Simulators*. Swets & Zeitlinger, Lisse, Netherlands, 1999.

[9] C. Esveld. *Modern Railway Track*. Delft University of Technology, Delft, Netherlands, 2001.

[10] F. Braghin, R. Lewis, R.S. Dwyer-Joyce and S. Bruni. A mathematical model to predict railway wheel profile evolution due to wear. *Wear*, **261**, 1253–1264, 2006.

[11] T. Telliskivi, U. Olofsson. Wheel-rail wear simulation. *Wear*, **257**, 1145–1153, 2004.

[12] R. Enblom and M. Berg. Simulation of railway wheel profile development due to wear: influence of disk braking and contact environment. *Wear*, **258**, 1055–1063, 2005.

[13] MATLAB® Official Web Site. Available at: http://www.mathworks.com.